

# Digitize Your Body and Action in 3-D at Over 10 FPS: Real Time Dense Voxel Reconstruction and Marker-less Motion Tracking via GPU Acceleration

Jian Song\*, Yatao Bian\*<sup>1</sup>, Junchi Yan, Xu Zhao, Yuncai Liu

Department of Automation, Shanghai Jiao Tong University, and Key Laboratory of System Control and Information Processing, Ministry of Education of China, Shanghai 200240, China

## Abstract

In this paper, we present an approach to reconstruct 3-D human motion from multi-cameras and track human skeleton using the reconstructed human 3-D point (voxel) cloud. We use an improved and more robust algorithm, *probabilistic shape from silhouette* to reconstruct human voxel. In addition, the annealed particle filter is applied for tracking, where the measurement is computed using the reprojection of reconstructed voxel. We use two different ways to accelerate the approach. For the CPU only acceleration, we leverage Intel TBB to speed up the hot spot of the computational overhead and reached an accelerating ratio of 3.5 on a 4-core CPU. Moreover, we implement an intensively paralleled version via GPU acceleration without TBB. Taking account all data transfer and computing time, the GPU version is about 400 times faster than the original CPU implementation, leading the approach to run at a real-time speed.

## 1 Introduction

Visual information based human motion analysis is an important research direction in computer vision. And 3-D human motion reconstruction and tracking is one of the most challenging tasks. There are huge applications of the related techniques, ranging from virtual realization, film animation, intelligent surveillance, high level human machine interaction, video transmission and compression to sports and medical treatment. With the rapid development of hardware facilities and the theory of computer vision, currently, building a video based human motion construction system for real application is attracting more and more attentions from both academic and industrial fields. Considering the intensive computational demand, GPU will definitely play a very important role in this campaign. This is also the reason why we make our best to take part in this contest.

The main task of 3-D human motion reconstruction is to estimate the motion parameters and body configuration of 3-D human body model, by utilizing visual information from multiple cameras. It also means that we aim to get the position and the configurations of human body parts in real 3-D world. Due to the complexity of this problem, the computational complexities of related algorithms are impermissible to a real-time implementation in CPU. Therefore, the algorithm acceleration using GPU is a nice choice. Nowadays, GPU is getting its wide recognition and application

---

<sup>1</sup> \* denotes equal contribution

among scholars, especially in the 3-D reconstruction field. A latest relevant case is the work presented by Jan-Michael Frahm et al. from UNC, who published their work on ECCV (European Conference on Computer Vision) [3]. They collected the photos from internet (millions of images), thanks to GPU for acceleration, they successfully reconstruct the city of Rome in one day, without the help of cloud computing. In comparison, Sameer Agarwal from University of Washington achieve such performance in their ICCV (International Conference on Computer Vision) paper, owing to the high performance from cloud computing (62 workstations), and the number of images they approach is only 150,000, significantly fewer than the work [3]. From above cases, one can get a clear perspective that GPU is playing very important role in computer vision field.

In our project, there are two classes of core techniques: **3-D voxel reconstruction of human body** and **3-D body pose tracking**. Both of them are time consuming. For 3-D voxel reconstruction, the main algorithm is Shape From Silhouette (SFS). Regarding with SFS techniques, Sofiane Yous et al. leveraged the GPU's advantage in light tracking, and achieved the real time 3-D reconstruction in some published datasets [5] in 2007. Moreover, Neal Orman et al implemented a free viewpoint rendering system thanks to the acceleration capability brought by GPU [6]. Compared with the traditional SFS methods, here we adopt the method proposed in [1][7] to achieve better robustness, which is insensitive to outliers, while at the price of computational inefficiency. And since we have not found any GPU based implementation of this method, we are exploring the potential high efficiency when GPU is adopted in this project.

After obtaining the 3-D voxel of human body, the next step is to perform human pose estimation and tracking. This is another time-consuming part of this project. In industrial field, 4D View Solution<sup>2</sup> works on 3-D pose estimation but mainly using parallel CPU. In our project, we select GPU as the accelerator. The core algorithm for pose tracking is Annealed Particle Filter (APF). Regarding with the APF based tracking approach, inherently it is a particle filter algorithm, which has a natural form of parallel computing and therefore it is expected to have a high potential in acceleration.

Towards the aim of 3-D human body voxel reconstruction and 3-D pose tracking, the presented project bears the following aspects:

- Using multiple cameras to obtain visual information of human motion in indoor environments.
- Using human skeleton model as the prior model of human body.
- Achieving generality to different types of human motion.
- Achieving quick and robust solution to 3-D human pose tracking.

In sum, the main algorithms in this project are listed as follows:

- For 3-D human body reconstruction, probabilistic shape from silhouette approach is implemented [1][7].
- For 3-D human pose tracking, annealed particle filter method is used [2].

---

<sup>2</sup> A start-up company is born out of Rhone-Alpes National Institute for Research in Computer Science and Control. <http://r24085.ovh.net/company.html>

We next will introduce these algorithms in detail.

## 2 Algorithm Design

### 2.1 System Flowchart

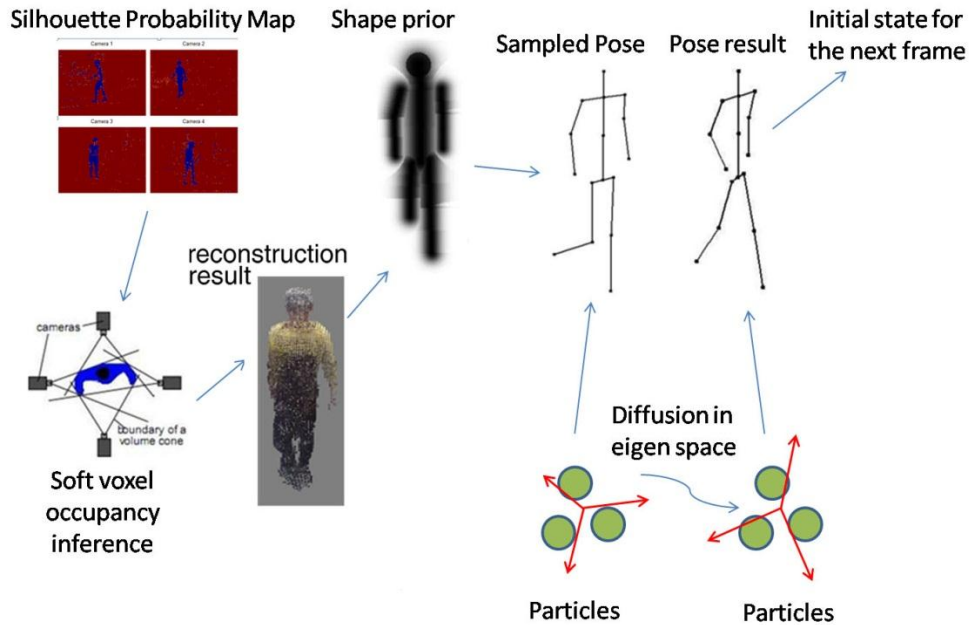


Figure 1 System flowchart

Figure 1 shows the system flowchart. For a given image, we first use *probabilistic shape from silhouette* (PSFS) [1][7] to get reconstructed voxel of human surface. Then with the information from reconstructed human body, we track human skeleton in an annealed particle filter [2] framework. We will give detailed descriptions of the two algorithm parts in the following sub chapters.

## 2.2 3-D Voxel Reconstruction

### 2.2.1 General Reconstruction Methods

Usually the two main methods used for reconstruction are based on silhouette and photometry. Photometry-based methods [9][10][11] are sensitive to camera registrations and have a quite high complexity. Silhouette-based methods are popular for use in multi-camera environments mainly due to their simplicity and computational efficiency.

Shape from silhouette [12][13] is a silhouette-based method that is well studied. It first gets the silhouette using a simple background subtraction method. Figure 2 shows how shape from silhouette works. As perspective projection suggests, the object in the scene should be located inside the three dimensional centrum formed by the camera center and silhouette. It is obvious that an object

can be reconstructed by carving a big region of interest with multi-view images taken from that object.

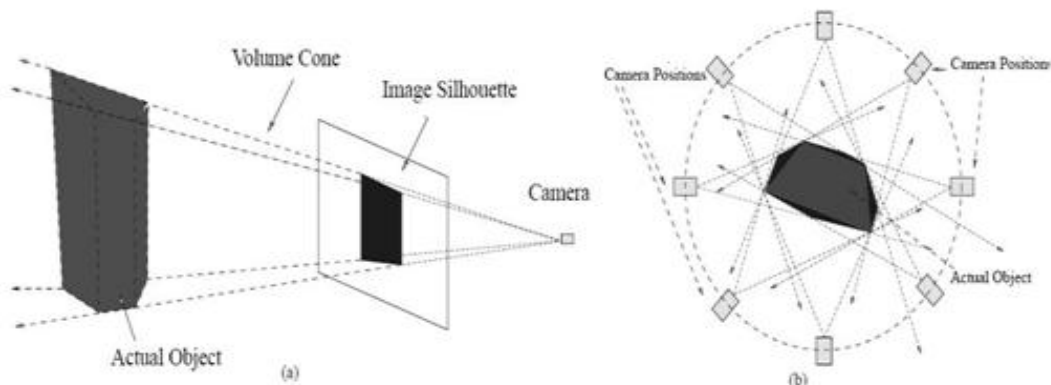


Figure 2 Generalization of 3-D Reconstruction algorithm [12]

### 2.2.2 Improved Scheme: Probabilistic Shape from Silhouette

We improved the original shape from silhouette. We use the visual hull of the human body as a basis of our algorithm. While very often silhouettes are used to infer shapes in a two-step process: an individual decision about silhouette occupancy is made on a per-view basis, and then shape is inferred geometrically from all available silhouettes using visual hull methods; yet here we infer the probability of each voxel occupancy by fusing the information from image cues in an incremental updating Bayesian framework as first proposed in the work [7] and further improved by our work [1]. The following algorithm is from our published paper [1].

In order to make full use of the image information from multi-views, we do not segment the binary silhouette of each image on the fly. Instead, we adopt a Bayesian framework to calculate the silhouette probability of each pixel. For a pixel  $p$  in image  $r$ , the posterior probability of representing foreground can be calculated by Bayesian theory:

$$P(\mathcal{F}_r^p = 1 | I_r^p) = \frac{P(I_r^p | \mathcal{F}_r^p = 1)P(\mathcal{F}_r^p = 1)}{\sum_{\mathcal{F}_r^p=0} P(I_r^p | \mathcal{F}_r^p)P(\mathcal{F}_r^p)} \quad (1)$$

where  $\mathcal{F}_r^p = 1$  indicates the pixel  $p$  in image  $r$  represents foreground, otherwise,  $\mathcal{F}_r^p = 0$ .  $I_r^p$  denotes the color feature vector of pixel  $p$  in image  $r$ . For simplicity, we model  $P(I_r^p | \mathcal{F}_r^p = 0) \sim N(I_r^p | \mu_r^p, \sigma_r^p)$ , a single Gaussian model. Since the foreground color information is unknown for the first frame, we assume the foreground obeys a uniform distribution:

$P(I_r^p | \mathcal{F}_r^p = 1) \sim U(I_r^p)$  We choose not to favor any pixel location by setting the prior term  $P(\mathcal{F}_r^p = 1) = P(\mathcal{F}_r^p = 0) = 0.5$ . And we obtain the silhouette likelihood map defined as:

$$SLM_r^p = P(\mathcal{F}_r^p = 1 | I_r^p) \quad (2)$$

Figure 3 shows silhouette likelihood map of four views from tow sequences. There are many holes and noises which cannot be removed using normal shape from silhouette method which results not perfect reconstructed voxels.

Consequently, given a set of images  $\{I^p\}_n = \{I_1^p, I_2^p, \dots, I_n^p\}$ , one can calculate the silhouette likelihood maps  $\{S^p\}_n = \{S_1^p, S_2^p, \dots, S_n^p\}$ .

Similar to the process of obtaining silhouette, given the silhouette likelihood map of multiple images  $\{S^p\}_n = \{S_1^p, S_2^p, \dots, S_n^p\}$ , we estimate the posterior probability representing occupancy of each voxel in volume of interest as follows:

$$P(V_i = 1 | \{S^p\}_n) = \frac{P(\{S^p\}_n | V_i = 1)P(V_i = 1)}{\sum_{V_i=0}^1 P(\{S^p\}_n | V_i)P(V_i)} \quad (3)$$

where  $V_i = 1$  denotes the voxel  $i$  is occupied by an object, otherwise,  $V_i = 0$ . The pixel of the silhouette likelihood map  $\{S^p\}_n = \{S_1^p, S_2^p, \dots, S_n^p\}$  is the projection of voxel  $V_i$ . The term  $P(\{S^p\}_n | V_i = 1)$  in Eq.(3) can be calculated in Eq. (4):

$$\begin{aligned} P(\{S^p\}_n | V_i) &= P(\{S^p\}_{n-1} | V_i)P(S_n^p | V_i) \\ &= \prod_{k=1}^n P(S_k^p | V_i) \end{aligned} \quad (4)$$

Then the problem of voxel occupancy inference is reduced to model the term  $P(S_k^p | V_i)$  ( $k = 1, 2, \dots, n$ ) Here we introduce a latent variable  $O_k^p$ .  $O_k^p = 1$  denotes there exists object occluding the voxel  $V_i$  on the viewing line connecting the voxel and its projection  $S_k^p$ , otherwise  $O_k^p = 0$ . Thus we get the following equation:

$$P(S_k^p | V_i) = \sum_{O_k^p} P(S_k^p | O_k^p, V_i)P(O_k^p) \quad (5)$$

For the term  $P(O_k^p)$ , we set  $P(O_k^p = 0) = P(O_k^p = 1) = 0.5$  indicating with no prior preference; for the term  $P(S_k^p | O_k^p = 0, V_i = 0)$  which indicates that there exist neither voxel  $V_i$  nor other object lying on the viewing line of pixel  $S_k^p$ , we have:

$$P(S_k^p | O_k^p = 0, V_i = 0) = 1 - SLM_k^p \quad (6)$$

For  $P(S_k^p | O_k^p = 1, V_i = 0)$ ,  $P(S_k^p | O_k^p = 0, V_i = 1)$ ,  $P(S_k^p | O_k^p = 1, V_i = 1)$ , which denote there at least exists one voxel lying on the viewing line, we assume:

$$P(S_k^p | O_k^p = 1, V_i = 0) = SLM_k^p \quad (7)$$

$$P(S_k^p | O_k^p = 0, V_i = 1) = SLM_k^p \quad (8)$$

$$P(S_k^p | O_k^p = 1, V_i = 1) = SLM_k^p \quad (9)$$

Finally we filter the probability of voxels occupied by human body and then perform a thresholding process, to remove voxels inside human body and get the surface voxels.

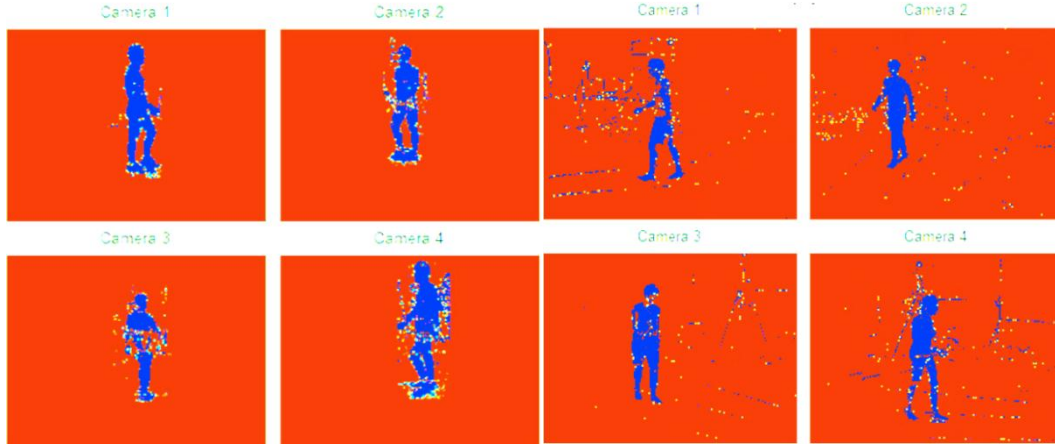


Figure 3 Silhouette likelihood map

a) from our dataset

b) from Brown University's dataset

## 2.3 Human Skeleton Tracking

### 2.3.1 Annealed particle filter

Particle Filter (PF) is based on Monte Carlo methods. It represents the probability distribution by particle set which can be used in any state space model. The main idea of Particle filter is to select random state particle from posteriori. This process is a sequential important sampling. In other words, PF is an Approximation Method for probability distribution function by finding a set of random sample in state space. Although the probability distribution is only an approximate for real distribution, it drops the limitation of random variables satisfying Gaussian distribution in nonlinear filter because of the non-parameter structure. Therefore the particle filter has wider and stronger modeling ability. The procedure of Particle Filter can be seen from Figure 4.

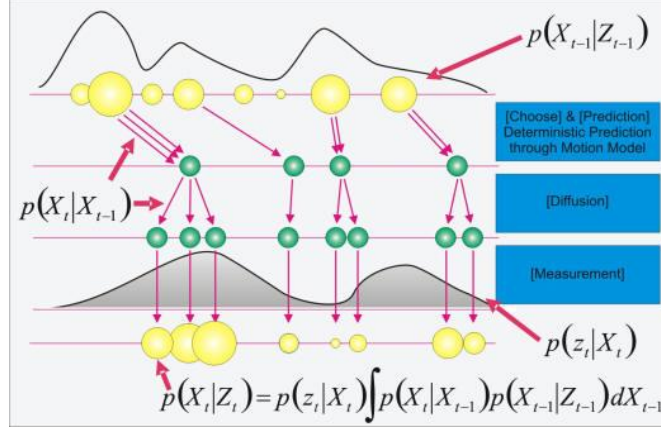


Figure 4 Particle filter iteration loop

### Simulated annealing

Simulated annealing is an approach for minimizing multivariate functions. The term simulated annealing derives from the roughly analogous physical process of heating and then slowly cooling a substance to obtain a strong crystalline structure.

The cooling schedule is to anneal the problem from a random solution to a good, frozen, placement. Specifically, we need a starting hot temperature (or a heuristic for determining a starting temperature for the current problem) and rules to determine when the current temperature should be lowered, by how much the temperature should be lowered, and when annealing should be terminated.

### Annealed particle filter

The process of Annealed particle filter (APF) [14] is stated as follow:

1. For every time step  $T_k$ , an annealing run is started at layer  $M$ , with  $m = M$ .
2. Each layer of an annealing run is initialized by a set of un-weighted particles  $S_{k,m}$ .
3. Each of these particles is then assigned a weight

$$\pi_{k,m}^i \propto \omega_m(Z_k, s_{k,m}^i) \quad (10)$$

which are normalized so that  $\sum_N \pi_{k,m}^i = 1$ , The set of weighted particles  $S_{k,m}^\pi$  has now been formed.

4.  $N$  particles are drawn randomly from  $S_{k,m}^\pi$  with replacement and with a probability equal to their weighting  $\pi_{k,m}^i$ . As the  $n^{th}$  particle is chosen it is used to produce the particle  $s_{k,m-1}^n$  using

$$s_{k,m-1}^n = s_{k,m}^n + B_m \quad (11)$$

where  $B_m$  is a multi-variant Gaussian random variable with variance  $P_m$  and mean 0.

5. The set  $S_{k,m-1}$  has now been produced which can be used to initialize layer  $m - 1$ . The process is repeated until we arrive at the set  $S_{k,0}^\pi$

6.  $S_{k,0}^\pi$  is used to estimate the optimal model configuration  $X_k$  using

$$X_k = \sum_{i=1}^N s_{k,0}^i \pi_{k,0}^i \quad (12)$$

7. The set  $S_{k+1,M}$  is then produced from using  $S_{k,0}^\pi$

$$s_{k+1,M}^n = s_{k,0}^n + B_0 \quad (13)$$

This set is then used to initialize layer  $M$  of the next annealing run at  $t_{k+1}$ .

### 2.3.2 Tracking Skeleton using Reconstructed Voxels

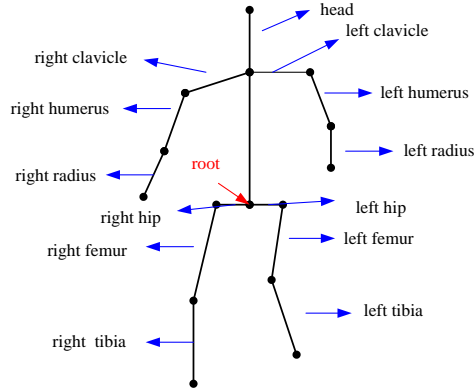


Figure 5 Human skeleton model

10 cylinders are set for different part of human body. The following table shows the corresponding part of the cylinders

1	TORSO
2	Left thigh (upper leg)
3	Left calf (lower leg)
4	Right thigh (upper leg)
5	Right calf (lower leg)
6	Left upper arm
7	Left lower arm
8	Right upper arm
9	Right lower arm
10	Head

Table 1 10 cylinders of human



We can get articular human model by setting base and bottom radius and length for each cylinder. This model has 31 degrees of Freedom, representing position and freedom of the ten cylinders.

Considering the 31 DOF of skeleton in one frame as a particle vector, and using the projection of voxels to be the prior knowledge, we can find an optimized particle and the get the new skeleton in the annealed particle filter framework. First we propagate the particles in the 31 dimension space. Each of the particles represents one pose of a skeleton. Then we match images generated by these particles and the projection of voxels in 2-D images and also their edges. We use the matched value as weight numbers for particles and we get a new particle after adding all these weighted particles. This new particle is then pushed into the next annealing layer. After propagating particles in all layers, we get the optimized particle, which represents the human skeleton in a new frame. Particle number is usually set to a value from tens to hundreds depending on the tracking condition. And the annealing layer is usually set to around 10.

### Particle Weight

Weight value in formula (10) is divided into two parts. One is from the edge information,

$$\sum^e(X, Z) = \frac{1}{N} \sum_{i=1}^N (1 - p_i^e(X, Z)) \quad (14)$$

And the other is from the silhouette,

$$\sum^r(X, Z) = \frac{1}{N} \sum_{i=1}^N (1 - p_i^r(X, Z)) \quad (15)$$

While we have multi-cameras in reconstruction and tracking, the final weight is a sum of that two parts from all cameras, that is

$$\omega(X, Z) = \exp - \left( \sum_{i=1}^c (\sum_i^e(X, Z) + \sum_i^r(X, Z)) \right) \quad (16)$$

Where C indicates the camera number

## 3 Algorithm Parallelization

### 3.1 Parallelism Analysis

Our scheme is based on computing and processing of images (digitized as matrix in practice), which has high parallelism to the task itself.

From the micro point of view, many intermediate processes are math operations of images or matrices. In the algorithm, large scale data is stored as continuous large array (2-dimensions or 3-dimensions). These math operations can be accelerated by GPU parallelization.

From the macro point of view, both reconstruction and tracking parts in our algorithm are the procedures of processing multi-camera information. These separate processes of each camera can be accelerated by parallelization.

The specific analysis is presented in the following sub chapters according to the nature character of reconstruction and tracking algorithm.

### **3.1.1 3-D Voxel Reconstruction**

The hot spot of 3-D reconstruction is the computation of voxel. And the color rendering is also an iterative process of all voxels.

Some parallelizable parts of the algorithm are listed as follows:

- Reconstruction problem is the procedure of analyzing 3-D space information after image processing, the data of which is multi-dimension matrix whose math operations has parallelism.
- Both reconstruction and color rendering are superposition of processing procedures of multi-cameras which are independent to each other and lead to parallelism.
- Reconstruction is the procedure of filtering all the voxels in three dimension region, the procedures for each voxel has nothing to do with others while the number of voxel is very large. Camera image information is processed in this procedure meanwhile. Great acceleration can be achieved via parallelization of voxel and image pixels processing.
- Color rendering aims to get color information by processing the reconstructed voxels. The large number of voxel and independence of each procedure for one voxel will largely contribute to acceleration via parallelization.

### **3.1.2 Human Skeleton Tracking**

The hot spot of human skeleton tracking lies in the weight assigning process.

Some parallelizable parts of the algorithm are listed as follows:

- Tracking problem is the procedure of analyzing matching degree between real world images and constructed images after image processing, the data of which is multi-dimension matrix whose math operations has parallelism.
- The particles' weights are computed by formula(10), which will have a significant acceleration due to the large number of particles and the independence of each weight computing procedure.
- In the procedure of assigning weight for one specific particle, formula(16) is a superposition process from several cameras. And the independence of each camera's processing leads to parallelism.

## **3.2 Parallellization on Multi-Core CPU**

To parallelize our program via GPU, we first parallelized it using multi-threads on multi-core CPU.

The parallelism on CPU is different with that on GPU since CPUs cannot hold as many threads as GPU running at the same time and the thread control is done explicitly. So we only paralleled the top level of all parallelizable parts.

We use Intel® Threading Building Blocks (Licensed under GPLv2 with the runtime exception) to build parallel programs on CPU.

In the voxel reconstruction part, we parallelized the calculating process of each camera while constructing voxels and rendering colors. And in the human skeleton tracking part, we parallelized the time-consuming process of each particle. These paralleled program parts are represented under the name of XXX\_Invoker.

### **3.3 Parallelization on GPU**

#### **3.3.1 Algorithm Restructuring**

GPU and CPU are adept in different computational demand scenarios because of architecture differences. Taking into account these differences and in accordance with the GPU computing features, we refined the algorithm structure. The overall frameworks of CPU and GPU algorithms are shown in the following figure.

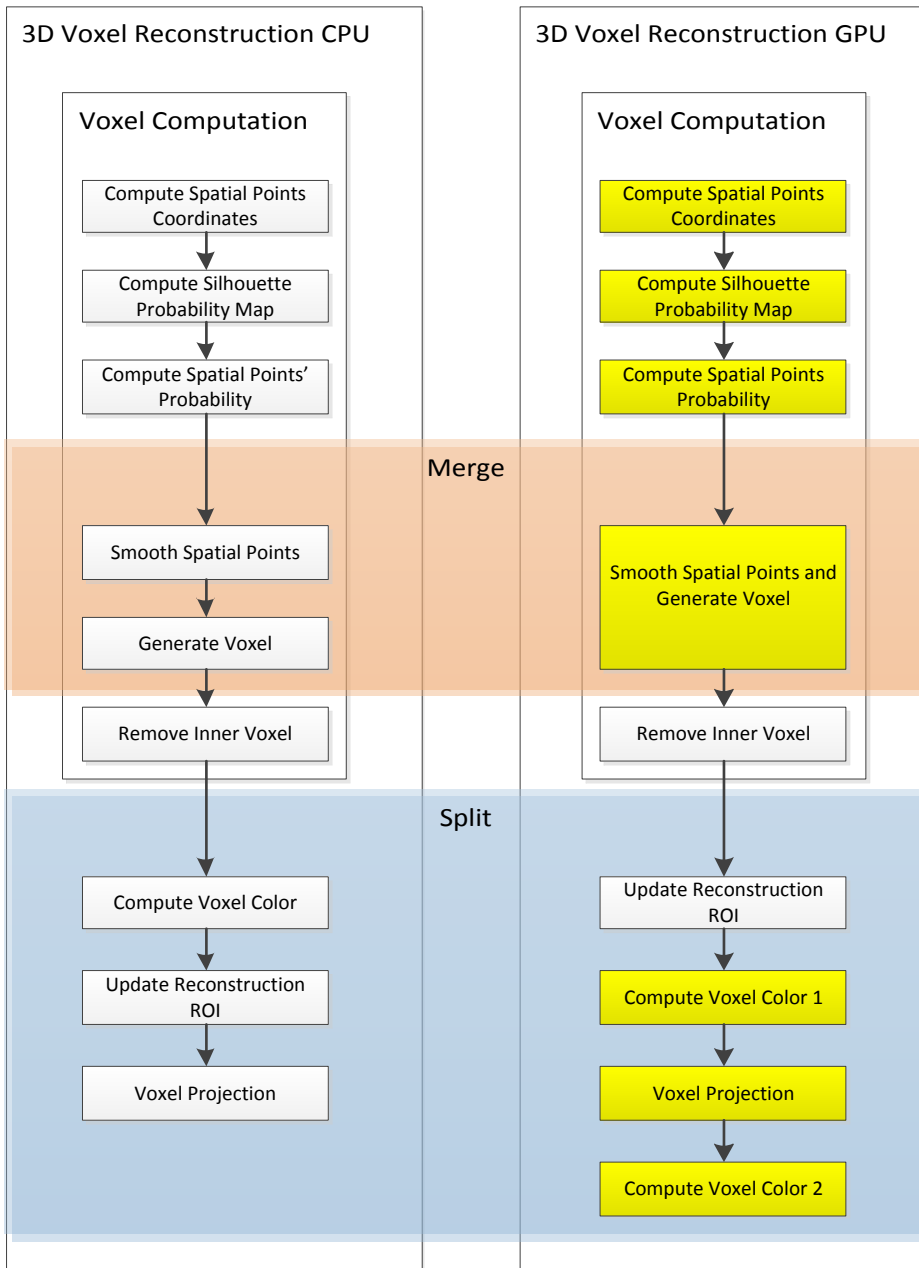


Figure 6 Comparison of CPU and GPU frameworks for 3-D voxel reconstruction algorithm

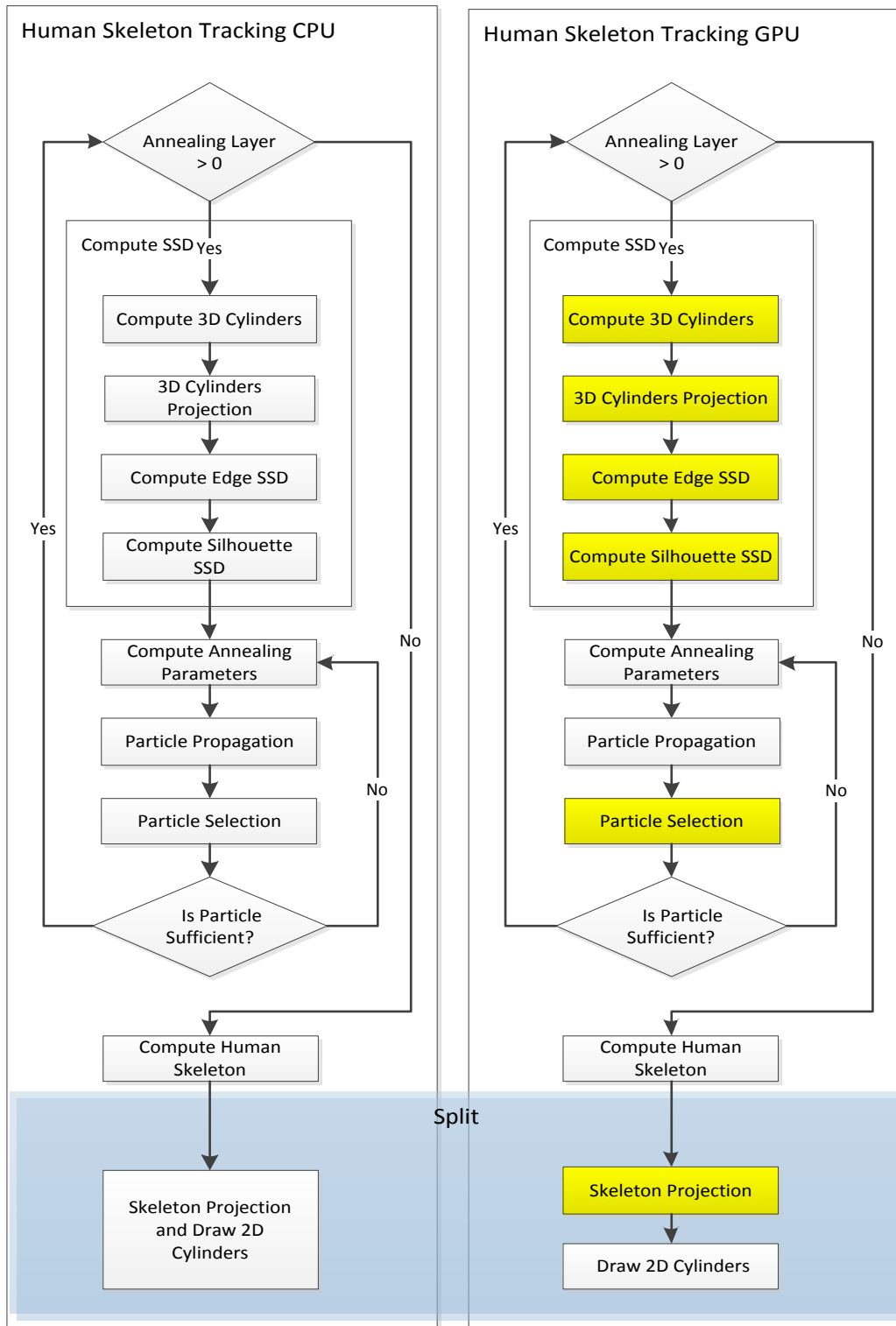


Figure 7 Comparison of CPU and GPU frameworks for human skeleton tracking algorithm

The comparisons of CPU and GPU algorithms are shown in Figure 6 and Figure 7, in which yellow background highlights GPU computing parts. For the parts which are more suitable for CPU processing, we modify interfaces and retain CPU implementation to achieve the overall optimum.

As shown in the figures, the algorithm has three major structural changes, that is, one merger and two splits.

- **Merging Spatial Points Smoothing and Voxel Generating**

In the spatial smoothing process, a float array with maximum length of 2250000 that is 8.6 MB of data is traversed and a new array with the same size is generated which is traversed later to generate filtered voxel cloud. Time complexity of each array traversing is same and memory copy is cheap when doing this on CPU. But for the sake of global memory access limitation on GPU, additional write and read operation of all the data in array will take much time when traversing the array twice other than once, so merging this procedure will significantly improve GPU computing efficiency.

- **Splitting Voxel Color Computation**

Voxel color calculation can be divided into two parts. Similar to the above analysis, the first half of which could share the same traverse process with voxel projection to reduce global memory access, and because of the different array lengths traversed in the first part and the second part, splitting will not increase memory access. So we split voxel computation into two parts handled by two kernels, respectively.

- **Splitting Skeleton Projection and 2D Cylinders Drawing**

In this step, the computed 3-D skeleton is projected to corresponding 2D planes of each camera and drawn to the images respectively. In CPU code, 2D cylinders on each image are drawn right after the end of computing skeleton projection in corresponding plane, while in GPU code, 2D cylinders on these images are not drawn until projection of all camera planes are completes. This is because projection computation can be parallelized on GPU and drawing on CPU does not spend lots of time. Moreover, drawing on CPU will refrain from two steps of large data copy.

### **3.3.2 Data Transfer Optimization**

Data transfer always takes a long time in GPU program. We use the unblock way to read or write data to GPU device, and use multiple commandqueues to deal with different operations.

Read/write operation is arranged to the same commandqueue when host program needs to read/write data from device and the data will be used by the following kernel or CPU code. And if the data read/write from device is not needed immediately, the operation is put into another commandqueue, and the operations need these data wait for the events from read/write operation.

This will parallelize the CPU computation, GPU computation and data transfer as possible, to hide the time spent on CPU by serial code and the time spent on transferring data between host and device. The timeline after optimization is shown in Figure 8.

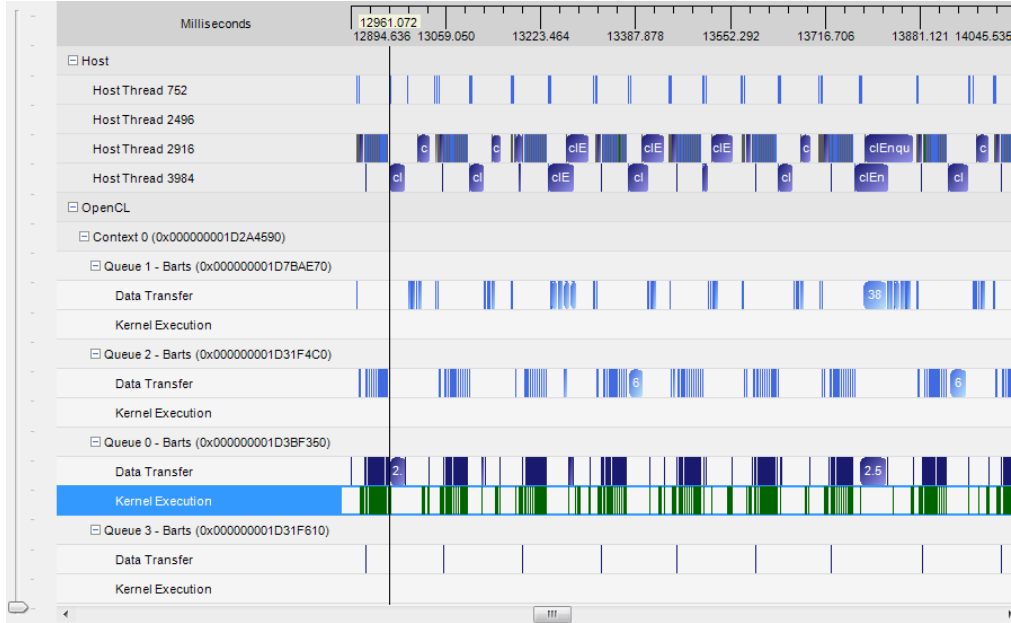


Figure 8 timeline after optimization

### 3.3.3 Main Program Optimization Voxel Computation

As shown in Figure 6 this computation has 5 steps. Let  $xlen$  (maximum value is 150) denotes sample numbers of x coordinate,  $ylen$  (maximum value is 150) denotes sample numbers of y coordinate,  $zlen$  (maximum value is 100) denotes sample numbers of z coordinate, and  $camNum$  denotes camera number in use(it is set to be 8 in the program).

- Compute spatial point coordinates. Compute spatial point coordinates using point location. Global work-item number is  $xlen * ylen * zlen$ , work-group size is set as  $(4, 4, 4)$ .
- Compute silhouette probability map. It is computed separately for each camera, global work item number is image's pixel number.
- Compute spatial points' probability. Compute points' probabilities using foreground probabilistic graph. The computation result for each camera is reduced using local memory. Global work-item number is  $xlen * ylen * zlen * camNum$ . Work-group size is  $(256 / camNum, camNum)$  and work-group number is  $(\lceil xlen * ylen * zlen / (256 / camNum) \rceil, 1)$ .
- Smooth spatial points and generate voxel. Global work-item number is  $xlen * ylen * zlen$ , and work-group size is  $(4, 4, 4)$ .
- Remove inner voxel. About 30000 numbers of surface voxel of human is sifted from a large amount of data with size of  $xlen * ylen * zlen * 8$ , which can be up to 18000000. This process is time-consuming on GPU so CPU implementation is reserved.

### Voxel Projection and Color Computation

To make full use of GPU resources, we changed the code structure of color computation. Because of the optimization of algorithm implementation, we reduced time complexity without disturbing the correctness of the procedure. So this part of algorithm has a great speed up after the whole optimization on GPU. As shown in Figure 6, procedures in CPU program are split and disordered

into 3 steps after optimization. The global work-item number is  $xlen * ylen * zlen * camNum$  in the first step and equals to image pixel number in the following two steps.

### Compute Sum-squared Difference (SSD)

This part takes most of the time in skeleton tracking algorithm and has the most parallelism as well. As shown in Figure 7, it has 4 specific steps. Let *cylNum* denotes cylinder number (10 in the program), *camNum* denotes camera number (8 in the program), *particeNum* denotes particle number (can be adjusted according to different data, 200 for test data).

- a) Compute Spatial 3-D Cylinders. Ten cylinders' spatial locations and orientations are computed according to the 31 parameters of each particle. The global work-item number is set as *particleNum*.
- b) 3-D Cylinders Projection. Project spatial 3-D cylinders to the corresponding 2D plane of each camera. Global work-item number is  $particleNum * camNum * cylNum$ . One specific work-group is in charge of computation of one particle, work-group size is  $(camNum, cylNum)$ , and work-group number is  $(particleNum, 1)$ .
- c) Compute Edge SSD. Edge SSD is computed using cylinder projections on 2D planes and edge maps. Global work-item number is set as  $particleNum * camNum * cylNum * 2$ . The computation of one specific particle lies in one work-group, and then data reducing is issued using local memory. The work-group size is  $(camNum, cylNum, 2)$ , and work-group number is  $(particleNum, 1, 1)$ .
- d) Compute Silhouette SSD. Silhouette SSD value is computed using cylinder projections on 2D planes and silhouette maps. Global work-item number is  $particleNum * camNum * cylNum$ . One specific work-group is in charge of computation of one particle, local memory is used to reduce data. The work-group size is  $(camNum, cylNum)$ , and work-group number is  $(particleNum, 1)$ .

### 3.4 Parallelization Result and Performance Analysis

- IDE  
Microsoft Visual Studio 2008, 32 bit MSVC compiler
- 3rd Party Library  
OpenCV 2.3RC  
  
QT Library 4.7.3  
  
Intel TBB3.0 update 7
- Test Environment  
CPU: Intel(R) Core(TM) i7 CPU 860 @ 2.80GHz  
  
RAM: 4.00G DDR3  
  
GPU: AMD Radeon HD 6870  
  
Driver date 2011/7/7, version 8.872.0.0  
  
OS: Windows 7 x64 Enterprise SP1  
  
OpenCL 1.1 AMD-APP-SDK-v2.5 (684.213)



CAL 1.4.1457 (VM)

- Test Data and Algorithm Parameters

Data: PEAR Dataset, Subject1\_Walk1\_Validate, 200 frames

Particle Number: 200

Annealed Layer Number: 10

We have implemented the CPU version, CPU + TBB parallel version and GPU version of algorithms, and following paragraphs compare these algorithms to evaluate the performance of GPU acceleration.

Because of the algorithm overlapping in optimization, we are not able to evaluate our algorithms individually. The following analysis takes the whole algorithm procedures into account, including voxel reconstruction, voxel color computation and human skeleton tracking.

TBB is a tool similar to OpenMP, the algorithm paralleled with TBB is essentially the same with the one not using TBB. The only difference is that TBB will automatically create numbers of threads when calculating for loops according to different CPU core number in runtime. Acceleration is achieved by using all available CPU cores. TBB is not used in the GPU accelerated algorithm, as all parallelism is performed on GPU.

In the code submitted in preliminary contest, the default algorithm running on CPU is the CPU+TBB version, which is paralleled using TBB. And due to the sake of automatically assigning threads according to the numbers of CPU cores in TBB, the runtime speed can change exponentially in this version of program when using different CPUs, especially those with different numbers of cores. This time change is not linear because not all parts of the algorithm are calculated using TBB. We use a 4-core Intel CPU to test the TBB-paralleled algorithm, and the result is used to illustrate relative acceleration of GPU program.

	Time 1(ms)	Time 2(ms)	Time 3(ms)	Average (ms)
CPU	33948.37	33924.86	33759.48	33877.57
CPU+TBB (4 cores)	9605.077	9597.044	9593.483	9598.535
GPU(pre)	219.8729	217.0209	218.3901	218.428
GPU(final)	84.53274	85.58835	84.41453	84.845207

Table 2 average time per frame (results of 3 times of running)

Table 2 shows the average time consumed per frame of the algorithm running a total 200 frames. The table lists the result of running the algorithm for 3 times as well as the average value. Time consumed on GPU has two versions which represent the time of previously submitted program and the final program. More detailed values of the time cost by each frame can be found in Table 4 in the appendix.

The algorithm takes an average of more than 30 seconds per frame on CPU, while the GPU speed up to about 200 milliseconds per frame, which is close to real time. For scenes with non-violent movements (such as walking), the speed of 200 milliseconds per frame or 5 fps is rather a real-time performance.

The specific acceleration ratios can be computed from Table 2, which are listed in Table 3.

	Acceleration Ratio (pre)	Acceleration Ratio (final)
CPU+TBB (4 cores) / CPU	3.5295	3.5295
GPU / CPU+TBB (4 cores)	43.9437	113.1300
GPU/ CPU	155.0972	399.2868

Table 3 Acceleration ration of the algorithm

CPU program parallelized using TBB on 4-core CPU has an acceleration ratio of 3.5, which varies with CPU core numbers.

In the previously submitted program, the acceleration ratio of GPU program compared to CPU program parallelized using TBB on 4-core CPU is a speed up of 44 times, varies with CPU core numbers as well. And the GPU program speeds up about 155 times compared to the original CPU program without TBB parallelism.

The final version of algorithm has an acceleration ratio of GPU program compared to CPU program parallelized using TBB on 4-core CPU of 44 times, varies with CPU core numbers as well.

The final GPU program speeds up about 399 times compared to the original CPU program without TBB parallelism.

## 4 Prospect

Kinect, a latest product brought out by Microsoft (refer [8] for algorithm details) is one of the paragons for the commercialization of such technique. On the other hand, the startup companies like the “4D View Solution” as mentioned in the previous context are trying to provide the end to end solutions to customers, which to some extent prompt its application in animation, communication, sports and surveillance and such. Based on the existing solutions and methods, one can observe that this technology exhibits a bright prospect based on a solid theory, while the high performance computing platform is still under its infancy. We have tested our reconstructing and tracking algorithm on PEAR database, which originally consumed a lot of time and now has been accelerated to real-time via GPU. Our algorithm running on multi-camera systems or Kinect systems can play a role in animation, communication, surveillance and such areas.

## References

- [1] Junchi Yan, Yin Li, Enliang Zheng, Yuncai Liu: An accelerated human motion tracking system based on voxel reconstruction under complex environments. Asian Conference on Computer Vision. (2009)
- [2] Alexandru O. Balan, Leonid Sigal, Michael J. Black: A quantitative evaluation of video-based 3D person tracking. ICCCN '05 Proceedings of the 14th International Conference on Computer Communications and Networks.
- [3] Jan-Michael Frahm, Pierre Georgel, David Gallup, Tim Johnson, Rahul Raguram, Changchang Wu, Yi-Hung Jen, Enrique Dunn, Brian Clipp Svetlana Lazebnik, Marc Pollefeys: Building Rome on a Cloudless Day. European Conference on Computer Vision. (2010)
- [4] Agarwal, S., Snavely, N., Simon, I., Seitz, S.M., Szeliski, R.: Building Rome in a day. In: ICCV.

(2009)

- [5] Sofiane Yous, Hamid Laga, Masatsugu Kidode, Kunihiro Chihara: GPU-Based Shape from Silhouettes. Proceedings of the 5th international conference on Computer graphics and interactive techniques in Australia and Southeast Asia. (2007)
- [6] Neal Orman, Hansung Kim, Ryuuki Sakamoto, Tomoji Toriyama, Kiyoshi Kogure, and Robert Lindeman: GPU-Based Optimization of a Free-Viewpoint Video System. Electronic Letters on Computer Vision and Image Analysis 7(2):120-133, 2008.
- [7] Franco, J., Boyer, E.: Fusion of multi-View silhouette cues using a space occupancy grid. In: Proc. of ICCV 2005, Beijing, China, vol. 1, pp. 1747–1754 (2005)
- [8] Jamie Shotton, Andrew Fitzgibbon, Mat Cook, Toby Sharp, Mark Finocchio, Richard Moore, Alex Kipman and Andrew Blake: Real-Time Human Pose Recognition in Parts from Single Depth Images. Conference on Computer Vision and Pattern Recognition. (2011) CVPR'11 best paper award.
- [9] K. Kutulakos and S. Seitz. A theory of shape by space carving. IJCV, 38(3):199–218, 2000.
- [10] B. Goldluecke, M. Magnor. Space-time isosurface evolution for temporally coherent 3D reconstruction. CVPR2004.
- [11] G. Vogiatzis, PHS. Torr, R. Cipolla. Multi-view stereo via volumetric graph-cuts. CVPR2005.
- [12] G. Cheung, T. Kanade, JY. Bouguet, M. Holler. A real time system for robust 3D voxel reconstruction of human motions. CVPR2000.
- [13] Laurentini, A.: The visual hull concept for silhouette- based image understanding. PAMI 16 (1994)
- [14] J. Duetscher, A. Blake, I. Reid, "Articulated Body Motion Capture by Annealed Particle Filtering," cvpr, vol. 2, pp.2126, 2000 IEEE Computer Society Conference on Computer Vision and Pattern Recognition (CVPR'00) - Volume 2, 2000

## Appendix

Test results of running each algorithm 3 times.

frame	CPU (ms)			CPU + TBB (4 cores) (ms)			GPU (ms)		
	1	2	3	1	2	3	1	2	3
1	35600.5	35652.8	35513.9	10252	10255.6	10359.3	145.425	152.239	155.904
2	33641.8	33700.1	33526	9470.22	9486.45	9465.98	81.5151	80.5634	125.687
3	32839.9	32920.3	32742.7	9219.91	9252.42	9213.83	103.1	80.5452	87.0664
4	32906.7	32995	32810	9126.02	9112.35	9274.83	82.0401	70.1632	84.3146
5	33318.4	33375.6	33204.6	9325.89	9269.03	9330.55	68.9786	72.0247	72.4673
6	33937.3	33993.8	33826	9443.41	9358.85	9341.25	95.623	79.8255	97.72
7	34964.3	34996.6	34828.6	9556.24	9535.68	9492.39	86.9925	71.6262	119.297
8	34794.8	34836.6	34660.4	9503.72	9474.04	9622.65	58.1777	75.3865	137.875
9	34388.3	34414.5	34260.6	9409.42	9324.38	9356.72	79.9194	89.0019	82.4673
10	36161.4	36156.4	36014.8	9802.5	9958.93	9822.64	90.3793	92.695	79.4183
11	36471.5	36427.7	36290.7	9972.38	9936.55	9838.54	124.304	78.8492	103.324
12	34901.2	34903.5	34751.5	9450.02	9569.22	9540.04	79.0944	93.1318	77.7996
13	34684.8	34648.2	34480.4	9455.61	9445.71	9437.74	88.0074	94.6182	104.53
14	34504	34501.8	34335.1	9462.61	9421.62	9450.51	98.1382	80.0257	77.1069
15	33844.9	33832.5	33656.4	9305.92	9358.47	9362.19	111.705	76.4321	69.0757
16	32626.2	32625.8	32473.8	9057.59	8940.46	9098.72	114.074	82.9919	72.6897
17	32540.9	32532.1	32377.7	9027.06	9039.79	9022.08	62.7196	78.6232	106.246

18	32120.2	32021.1	31893.9	8907.06	8838.18	9029.99	76.5956	78.7993	76.1069
19	32425.7	32418.7	32265	9072.47	9186.75	9085.62	94.2722	74.8075	78.3129
20	33669.3	33657.4	33514	9342.12	9366.85	9448.53	71.1893	78.3585	78.8299
21	34603.9	34613.4	34451	9698.33	9789.87	9783.41	101.314	118.421	81.2375
22	35053.4	35039.6	34901	9815.35	9844.04	9747.45	90.0716	75.039	85.0408
23	34836.2	34859.5	34708.4	9803.59	9697.96	9719.41	67.96	83.2522	74.0328
24	34553.8	34566.8	34405.4	9648.14	9711.33	9743.52	83.5859	104.65	104.85
25	35706	35681.5	35536.8	10049.4	10070	9968.84	106.472	71.4232	114.139
26	34915.8	34904.8	34767.2	9960.92	9962.03	9759.04	77.8377	111.941	75.2556
27	34396.4	34386	34231.8	9655.25	9788.04	9785.4	59.7662	79.7767	100.407
28	33520.3	33520.9	33349.2	9573.41	9495.59	9551.05	80.724	75.1254	77.7019
29	32804	32794.6	32639.3	9376.93	9520.01	9582.51	90.9878	78.1525	79.1405
30	32780.7	32776.9	32594.6	9413.95	9441.96	9548.58	78.7108	110.502	78.8973
31	32763.6	32770.5	32609.8	9335.42	9400.15	9461.49	121.127	72.0608	75.6417
32	31668.6	31662	31515.8	9126.74	9224.86	9081.39	74.4544	80.1044	89.6454
33	31059.6	31048.4	30890.6	8929.74	8992.01	9005.34	78.487	75.077	81.1716
34	31227.6	31237	31064.8	9125.55	9133.15	9021.72	71.6378	79.8033	72.3871
35	30276.6	30288.6	30127.3	8765.8	8845.49	8767.27	59.6867	75.9556	68.8992
36	30735.7	30736.8	30575.8	8816.05	8888.65	8990.87	76.2438	55.8981	62.8557
37	31162.1	31135.4	30976	8861.47	9134.62	9491.66	90.3319	74.7857	73.2792
38	31974.9	31987.3	31833.8	9268.02	9486.73	9512.07	69.9381	77.7708	74.2322
39	31785.2	31773.7	31613.6	9347.38	9339.87	9366.08	78.7553	73.9125	115.611
40	33316.4	33318.4	33153	9484.22	9594.7	9647.29	72.7781	83.8038	69.5103
41	33031.3	33018.4	32860.7	9672.67	9693.39	9585.59	65.7062	77.7194	109.873
42	32427.5	32432	32280.9	9291.26	9108.74	9395.02	72.2306	108.33	70.5912
43	33426.2	33405.4	33254.2	9513.36	9478.82	9565.69	85.0861	69.3364	79.7916
44	34943.7	34937	34753.2	9843.74	9799.12	9978.72	91.9732	85.8407	117.604
45	36321.3	36315.5	36145	10286.6	10393	10197.7	96.4666	85.0218	68.9783
46	38029.6	38015.1	37876.8	10882	10650.4	10737.1	84.0445	73.2399	93.931
47	38452.1	38461	38284.3	10926.6	10795.9	10975.3	75.7749	72.3787	80.1562
48	38847.4	38826.7	38659.9	10757.8	10671.3	10713.3	73.7413	76.8528	84.3612
49	37603	37577.1	37422.5	10521.1	10553.6	10222.9	80.4699	88.5739	70.9303
50	37000.4	36992.7	36811.2	10353.3	10405.6	10385.3	79.9208	72.9923	71.4615
51	35987.8	35943.1	35770.6	10052.3	10048.2	10031.5	126.185	73.343	58.6751
52	34258.9	34224.1	34067.4	9601.21	9604.71	9561.01	85.3307	84.1939	82.6043
53	33064.5	33200.9	33025.5	9192.81	9263.89	9296.56	74.27	69.8468	84.5632
54	32897.2	33057.8	32922.4	9328.34	9240.47	9194.8	75.7702	104.494	109.212
55	33925	33887.9	33747.7	9447.58	9466.66	9402.81	74.4213	120.224	115.111
56	33860.7	33868.4	33713.3	9544.03	9552.05	9631.64	75.8697	94.4497	67.0709
57	34682.3	34659.9	34511	9874.57	9599.09	9825.64	120.497	81.7706	73.4324
58	35191.2	35158.3	35006.8	10185.1	10192.8	9988.62	119.73	81.0111	99.4036
59	34667.1	34612.1	34474.2	9993.62	9750.95	9736.79	109.874	66.6899	71.0681
60	33222.2	33191.5	33054.5	9208.42	9709.71	9485.01	83.9497	123.989	73.1895
61	32288.1	32267	32104.5	9313.55	9427.36	9300.34	95.3532	80.9776	56.2674
62	32492	32484.3	32308.7	9615.77	9542.18	9367.01	70.4252	101.233	93.1894
63	32550.5	32528.6	32371.4	9569.48	9296.49	9886.95	106.304	83.9963	85.1148
64	32507.7	32506.6	32357	9506.64	9553.2	9586.39	91.4752	75.9286	75.6708
65	32372.1	32367.6	32215.1	9535.09	9600.36	9392.11	89.3042	107.808	103.626
66	31496.4	31481.9	31333.2	8967.79	9122.01	9225.35	79.5738	79.9714	65.719
67	32481.2	32464	32305.3	9508.83	9569.94	9719.06	76.0145	97.7521	78.5882
68	33476.2	33459.6	33296.1	9577.65	9859.55	9828.11	72.0151	75.5104	103.743
69	33203.5	33181.2	33032.6	9796.9	9942.04	9582.99	96.0838	91.096	81.0757
70	31828.2	31793.4	31657.8	9240.18	9558.47	9267.62	91.6349	72.7586	72.5997

71	31188.2	31156.2	31002.1	9071.39	9280.09	9146.51	80.2595	105.284	72.3164
72	31683.3	31498.1	31360.1	9373.42	9127.2	9265.59	81.8104	116.5	70.2492
73	32543.2	32512.5	32387.6	9480.85	9372.52	9251.81	59.0028	73.5005	73.9734
74	32096.2	32066.7	31959.5	9219.26	9218.76	9449.79	78.9095	77.4059	70.4057
75	31511.5	31465.5	31314.4	9188.55	9120.31	9111.47	80.8563	99.5173	73.7051
76	31865.3	31853.8	31709.4	9233.38	9089.69	9268.59	83.5006	77.5593	69.737
77	32979.6	32977.2	32870.7	9544.74	9574.74	9562.96	74.8318	86.6898	90.8937
78	32667.4	32611.1	32494.1	9309.08	9314.98	9212.08	65.6737	102.47	79.061
79	32960.5	32892	32784.8	9624.06	9317.88	9397.76	85.8338	83.3021	125.238
80	34155	34125.9	33956.1	9656.97	9860.35	9630.47	86.5794	90.0931	67.9532
81	33706.4	33658.1	33531.2	9457.28	9705.61	9539.47	73.8343	92.6349	96.7703
82	34551.3	34510	34352.7	9707.29	9801.87	9812.67	75.3123	82.1235	79.3531
83	32927.6	32876.7	32741.9	9274.47	9430.79	9375.85	68.5239	59.4327	96.0615
84	31502.1	31447.6	31300	9034.32	9060.03	9004.95	85.6745	89.0974	61.2588
85	33020.6	33001	32834.1	9526.25	9363.36	9366.82	77.0768	82.5249	76.0012
86	33744.3	33623.8	33504.4	9579.51	9608.37	9672.01	120.279	75.2046	85.1272
87	33410.1	33404.4	33241.7	9415.11	9353.66	9495.11	72.4041	111.09	73.8079
88	34737.1	34689.2	34540.7	9775.95	9733.12	9750.64	91.0257	83.0072	72.7736
89	37060.8	37032.5	36888.3	10346	10583.8	10555.7	72.3589	80.6298	63.9352
90	37341	37301.4	37141	10330.6	10348.6	10250.7	71.4989	100.419	126.345
91	37261.7	37229.8	37109	10144.2	10332.2	10283.2	87.283	83.3692	78.6126
92	38923.4	38812.9	38656.4	10596.5	10651.8	10642.5	77.6095	83.2547	73.588
93	38461.8	38426.5	38286.8	10387.4	10514.7	10357.6	68.2553	74.6121	84.4276
94	37633.3	37600.7	37450.5	10221.6	10101.6	10127.8	70.5491	100.51	71.4571
95	38223.1	38183.3	38032.4	10265.6	10355.6	10359	86.0023	88.0482	86.6861
96	38832.4	38768.3	38600.1	10585.9	10517.5	10584.2	84.1626	104.914	82.5201
97	35965.8	35926.4	35784.8	9949.36	9963.97	9970.05	89.7399	114.61	75.6537
98	34907.1	34878.9	34707.1	9714.16	9505.28	9699.62	87.3428	85.7419	78.7934
99	33704.5	33637	33480.2	9461.26	9365.03	9382.82	82.0485	90.3793	92.8369
100	32883.6	32852.7	32686.9	9256.75	9154.32	9135.54	77.4516	60.055	90.2535
101	32465.6	32422.8	32292	9264.42	9213.85	9194.33	70.7562	81.1191	66.0676
102	32613	32579.9	32423.1	9196.7	9229.97	9214.47	102.307	128.318	70.9208
103	32291.4	32250.7	32115.1	9205.03	9051.55	9133.48	71.1966	77.1565	108.533
104	32609.8	32543.7	32395.4	9171.69	9201.56	9144.44	112.728	70.7742	62.1663
105	33079.6	32969.7	32847.3	9229.9	9170.76	9269.6	82.3781	86.0776	74.9796
106	33293.2	33278.3	33119.1	9323.55	9320.93	9358.31	72.9601	102.069	71.0962
107	32607.4	32539.5	32384.1	9047.67	9253.64	8946.29	72.4551	96.0951	69.9521
108	31920	31884	31718.7	9061.82	9002.48	9125.16	79.7896	81.2776	70.3561
109	30527.7	30511	30368.3	8518.69	8659.65	8542.84	140.959	80.939	76.6727
110	31119.8	31110.8	30941	8830.54	8800.78	8760.15	104.741	117.999	73.3817
111	31180.4	31158.6	31005.9	8842.46	8733.13	8709.92	81.2049	70.6025	61.3215
112	30995.6	30955.7	30790.2	8604.25	8731.63	8756.32	79.0397	82.818	95.9952
113	31067.6	31031.4	30863.6	8848.25	8889.48	8787.71	130.641	104.967	80.2853
114	31028.9	31025.7	30839.8	8898.08	8813.58	8728.41	94.7039	69.566	69.8927
115	31152.1	31095.4	30913.4	8899.61	8909.59	8828.28	77.3925	105.244	116.389
116	31280.5	31251.5	31073.3	8967.47	8993.1	8987.81	77.8781	72.7014	75.6526
117	31773.5	31737.2	31560.5	9172.51	9152.94	9151.95	89.5528	77.7744	79.9852
118	31756	31735.1	31552	9179.07	9218.74	9181.63	75.6185	72.1913	77.279
119	31564.8	31516.9	31342.7	9099.27	9172.31	9121.55	67.7711	72.8709	123.153
120	32980.4	32945.7	32781.9	9782.39	9628.33	9552.71	78.0772	63.4178	70.7473
121	32295.7	32263.6	32116.8	9495.12	9451.08	9618.83	71.8674	78.784	76.5287
122	32614.5	32586.9	32436.8	9548.09	9654.34	9479.96	111.471	106.218	73.3011
123	32611.5	32572.1	32419.8	9755.21	9660	9497.57	75.2361	81.4275	83.9423

124	32493.6	32450.6	32270.9	9491.3	9619.31	9341.97	58.3546	66.6017	70.9562
125	32381.3	32323.4	32155.9	9685.26	9671.44	9678.93	80.1297	77.4503	70.3809
126	31769.3	31728.2	31558.1	9567.76	9465.09	9649.87	83.5385	110.177	80.9889
127	32645.2	32604.2	32427.8	9594.68	9605.59	9594.27	87.9684	137.323	75.9928
128	32637.7	32610.6	32424.1	9271.57	9544.22	9594.95	72.9083	59.5581	80.2649
129	32830.1	32790.4	32609.9	9362.45	9870.55	9500.13	68.6453	86.1301	77.9677
130	32288.6	32297.2	32098.9	9144.07	9663.86	9377.78	78.1866	74.5082	72.4524
131	32927.9	32936.9	32712.2	9669.63	9492.67	9519.01	73.0888	75.2917	66.9214
132	33934	33839.2	33657.6	9436.02	9540.87	9776.29	81.0466	73.0969	81.0378
133	35150.2	35122.6	34960.5	10319.7	10056.3	9794.28	74.146	59.9033	83.4841
134	34581.3	34548.9	34379.8	9990.77	9720.92	9590.98	66.9756	82.9215	120.903
135	34787.3	34745.2	34594.3	10056.7	9672.89	9841.61	70.7683	76.6632	78.8222
136	34629.5	34642.9	34451.8	9589.41	9687.03	9480.16	74.7727	119.406	120.548
137	35615.7	35616.8	35413.5	10107.2	9696.28	9815.82	106.854	76.198	77.8816
138	35248	35235.9	35069.9	9798.69	10010.2	9950.97	77.5734	65.5659	75.5586
139	36444.2	36407.5	36264.4	9932.79	9954.49	10156.4	98.5388	73.1053	116.89
140	38475.7	38460.3	38315.8	10486.6	10345.8	10449.2	87.8878	71.6711	124.432
141	38826.3	38810.5	38641.2	10808.7	10684.2	11047.5	83.6898	76.0697	58.4757
142	38667.7	38664.8	38486.2	10699	10869.7	10830.7	75.3786	78.2389	87.8641
143	37816.8	37806.7	37602.2	10815.6	10560.6	10323.1	116.186	63.7769	79.201
144	36781.1	36781.3	36577.8	10342.3	10469.5	10506.8	80.0685	87.9742	76.6946
145	36391.6	36340.1	36114.9	10190	10012.8	10244.5	77.1224	101.829	103.296
146	35727.6	35696.5	35500.5	9840.16	10072	10055.2	65.6336	108.198	80.7672
147	35243.6	35241.7	35036.7	9944.68	10002.6	10175.2	81.5472	100.31	93.2302
148	34713.5	34704.9	34511.1	9712.35	9777.54	9840.58	94.2168	103.486	89.1178
149	35782.2	35739	35556.6	10267.6	9776.74	9879.22	116.739	79.3038	86.6274
150	36870.3	36829.5	36660.3	10381.4	10456.3	10260.4	82.0018	83.9606	78.9108
151	35884.3	35872.6	35668.5	9893.97	9919.35	9975.89	97.7659	89.0701	80.0159
152	35362.5	35320.3	35112.6	10082.2	9818.4	9828.3	78.1016	79.543	74.0784
153	35543.2	35573.5	35335.2	10181.6	10066.5	10062.8	81.2862	82.5712	72.3033
154	33883.7	33862.4	33671.5	9729.62	9581.49	9651.09	107.016	70.9569	106.169
155	34031.4	34006.4	33828.7	9655.93	9644.88	9618.74	104.75	83.1457	83.4334
156	34603.5	34585.7	34402	9789.67	9553.68	9785.04	135.744	62.4127	81.725
157	34177	34176.6	33996	9508.7	9409.59	9292.89	71.4183	74.8174	90.5608
158	33388.2	33377.8	33207.3	9275.76	9255.48	9025.49	73.8011	77.6775	72.8188
159	33793.3	33729.9	33564.8	9177.4	9411.85	9524.19	74.3086	87.6825	99.7467
160	33525	33527.5	33340.2	9346.66	9418.04	9181.44	90.7198	90.6618	95.3375
161	34252.3	34240.7	34065.6	9521.23	9332.23	9402.89	90.1114	101.626	77.9615
162	35154.7	35110.9	34925	9817.59	9692.39	9767.24	72.9386	87.8878	95.9361
163	34214.1	34212.5	34014.6	9523.71	9318.69	9387.01	71.543	80.4563	86.2268
164	35573.7	35568.8	35354.3	9751.06	9750.57	9704.39	79.4225	109.075	108.197
165	34800.4	34757.5	34530.4	9620.65	9609.85	9631.02	78.6664	79.4591	99.2155
166	34183	34180.9	33990.4	9534.36	9531.32	9570.82	76.678	67.7989	80.5824
167	34003.7	33977.3	33814.1	9598.1	9334.95	9508.76	64.1925	81.0425	77.2801
168	34070.4	34055.4	33877.4	9591.54	9536.41	9526.37	79.4436	87.1586	77.8809
169	33224.6	33208.6	33012.6	9220.73	9297.34	9322.78	87.5634	101.634	86.9373
170	33483	33358.4	33159.4	9431.6	9173.08	9189.25	88.6855	74.7361	75.4255
171	34615.1	34604.5	34441.3	9462.98	9628.39	9442.95	69.5262	58.8373	76.7077
172	34720.6	34686.2	34526.7	9594.76	9373.74	9397.32	73.2481	75.6333	111.174
173	34726.5	34683.2	34488.3	9687.58	9535.6	9602.04	73.7446	84.7765	70.912
174	35096	34925.1	34722.9	9512.11	9680.85	9558.86	126.667	73.0773	73.1513
175	35652.7	35624.7	35450.4	9912.82	9714.58	9776.43	74.8208	88.4762	61.9213
176	35404.3	35379.9	35191.3	9696.16	9693.73	9748.5	75.115	79.228	70.1406

177	35859	35827.6	35634.4	9978.46	9839.39	9910.85	120.921	81.963	71.0025
178	34434.8	34416.4	34213.4	9584.53	9633.77	9517.88	88.7891	111.574	82.7604
179	34040.8	33897.8	33707.6	9394.67	9291.61	9198.92	94.6704	78.392	75.8258
180	33710.7	33710.2	33514.2	9574.77	9442.56	9346.1	59.9033	76.7708	124.525
181	33249.5	33113.5	32925.1	9327.29	9335.31	9230.34	80.1228	119.917	89.8966
182	33442.2	33404.4	33220.5	9398.64	9317.44	9378.29	90.2083	75.4011	75.6344
183	34352.9	34271.5	34061.7	9746.24	9683.05	9832.89	81.895	126.98	109.449
184	34484.9	34452.1	34271	9844.01	9772.22	9716.8	94.3287	90.719	74.0656
185	34416.2	34320.7	34126.2	9641.81	9795.28	9718.13	122.258	105.543	79.1438
186	35908.5	35901.7	35701.1	10247.8	10124.1	10209.1	78.5996	72.4899	71.2387
187	35175	35131.1	34947.1	10088.8	10034.5	9962.42	110.584	83.1311	93.4676
188	35454.3	35376	35182.9	10008	9991.53	10107.4	79.292	101.74	71.3823
189	35021.7	34998.1	34801.8	10027.6	9870.78	9950.72	76.0287	76.295	101.45
190	33625.1	33574.9	33570.1	9522.63	9484.14	9531.37	61.9066	110.437	79.1051
191	33374.6	33324.3	33155.5	9501.46	9490.54	9551.4	69.0803	71.7706	81.9514
192	34185.4	34161.1	33978.4	9867.9	9601.94	9919.46	73.1044	118.437	75.7955
193	34063.9	34042.9	33847.3	9784.25	9837.59	9781.06	74.2521	73.7076	75.6847
194	32426.6	32406.5	32234.9	9359.52	9350.86	9416.13	65.6584	63.5487	72.7721
195	33487.6	33495	33331.3	9751.73	9793.88	9788.08	75.9995	92.547	119.086
196	34401.5	34372.5	34240.9	10012.2	9986.84	9762.91	120.223	74.6165	119.039
197	33440.9	33431.3	33246.5	9878.34	9724.13	9506.84	69.5229	86.3091	82.1687
198	32560.6	32561.7	32393.4	9553.09	9578.07	9457.74	63.9314	80.4358	81.1927
199	31543.9	31521.3	31320.8	9226.17	9274.09	9232.85	74.7483	71.0557	71.052
200	30689.9	30657.3	30520	9071.56	8989.1	8960.14	90.2441	125.848	103.54

Table 4 time of each frame (results of 3 times of running)